Effects of sintering temperature on the phase developments and mechanical properties ifon clay

Fatai Olufemi ARAMIDE

Department of Metallurgical and Materials Engineering, Federal University of Technology, P.M.B. 704, Akure, Nigeria.
E-mails: foaramide@futa.edu.ng, fat2003net@gmai.com
* Corresponding author, phone: +2348038509288

Abstract

Effects of sintering temperature on the phase development and mechanical properties of clay based ceramics produced from Ifon clay (from Ondo State, Nigeria) were investigated. Clay sourced from the deposit was processed through hydrometallurgical means. The processed dried clay powders were uniaxially compacted into standard sample dimensions and fired at various sintering temperatures, 800°C, 900°C, 1000°C, 1100°C and 1200°C and held for 1 hour in a furnace. Both the raw processed clay and the sintered samples were characterized using state-of-art-equipment. The mechanical properties of the sintered samples were also investigated and the generated data analyzed. It was observed that the raw Ifon clay contains 5.63% kaolinite, 3.81% muscovite/illite, 30.9% microcline, 18.22% plagioclase/albite and 41.42% quartz. The apparent porosity, cold crushing strength, absorbed energy and water absorption of the samples decreased with increased sintering temperature, while the bulk density and Young's Modulus of elasticity of the samples increased with increased sintering temperature. The sintered samples were composed mainly of quartz, microcline and anorthite and only the sample sintered at 800°C contains muscovite. It was concluded that the sample which was sintered at 800°C held for 1 hour and cooled in the furnace

have the optimum properties.

Keywords

Sintering Temperature; Feldspar; Clay-based ceramics; Phase composition

Introduction

It is a well known fact that clays are important industrial raw materials, they are used almost as-mined in the fields of ceramics, paper, paint, petroleum industry, catalysis etc. [1, 2]. Their area of applications depends significantly on their structure, composition, and other physical attributes. The knowledge of these characteristics can help for a best exploitation and eventually may open-up new areas of application [3]. The properties of clay based ceramics depend on the characteristics, mineralogical composition of the parent clay and the processing conditions [4, 5].

Many researchers have worked on similar topics on fired ceramic bodies: Martín-Márquez *et al.* [6], investigated the effects of firing temperature on the properties of porcelain stone ware tile; Johari *et al.* [7], examined the effect of the change of firing temperature on microstructure and physical properties of clay bricks, while Aramide, [3], investigated the effect of firing temperature on mechanical properties of fired masonry bricks produced from ipetumodu clay. In all of these studies, the researchers only considered the firing temperatures as they affect the properties of their samples while the neglected the phases developed in the ceramic bodies during sintering. Aramide [8] has also reported on the effects of saw dust admixture on the physical/mechanical properties of clay based ceramic produced from the same clay deposit as those being considered in these article, it is entirely from different perspective.

Clay bodies undergo several changes during firing/sintering as a result of physical, chemical and mineralogical modifications which lead to development of new phases in the sintered ceramic products. The phase development is dependent on some parameters such as the mineralogical phase composition of the raw materials used for the preparation of ceramic mixtures and the temperature at which the ceramic body is sintered or fired.

The aim of this work was to explore the effects of sintering temperatures on the phase evolutions in the ceramic produced from Ifon clay deposit (in Ondo State, Nigeria) and

mechanical properties of the ceramics in order to optimize firing cycles for the production of ceramics of optimum properties.

Material and Method

Clay samples used in this work were sourced from Ifon, Ondo State in the south western part of Nigeria. The clay samples were collected according to ASTM D4220M – 14. The clay samples were first soaked in water for three days to dissolve the deleterious materials in them and at the same time to form slurry. The slurries were then sieved to remove deleterious materials and other foreign substances. The sieved slurries were then allowed to settle down for three days after which the clear floating water was decanted. The dispersed fine clays in water (clay slurries) were then poured into plaster of Paris (P.O.P) moulds and left undisturbed for three days in order to allow the remaining water to drain out completely. The resulting plastic clay masses were sun dried and subsequently dried in a laboratory oven at 110°C for 24 hours. The resulting dried clay samples were crushed and milled in a Rawwley Sussex grinder to an average particle size of 300μm.

The compounds present in the sample were determined by x-ray fluorescence (XRF). The results obtained are presented in Table 1. The mineralogical phases present in the samples were also determined using x-ray diffractometry (XRD). The phases present in raw clay are reported in Figure 1 and Table 2. The phases present in sintered ceramics are reported in Table 4.

The clay powders were compacted uniaxially into standard sample dimensions for cold crushing strength, bulk density, apparent porosity and water absorption. The resulting green compacts were fired at different temperatures ranging from 800℃ to 1200℃, soaked for 1 hour and allow cooling inside the furnace. The sintered samples were then characterized for various mechanical properties as described below.

Testing

Apparent Porosity

Test samples from each of the ceramic composites were dried out for 12 hours at 110°C. The dry weight of each fired sample was taken and recorded as *D*. Each sample was

immersed in water for 6 hours to soak and weighed while being suspended in air. The weight was recorded as *W*. Finally, the specimen was weighed when immersed in water. This was recorded as *S*. The apparent porosity was then calculated from the expression:

$$p=100*(W-D)/(W-S)*100 \quad (1)$$

The results obtained are presented in Table 3.

Cold compression strength, modulus of elasticity and absorbed energy

Cold compression strength test is to determine the compression strength to failure of each sample, an indication of its probable performance under load. The standard ceramic samples were dried in an oven at a temperature of 110°C, allowed to cool. The cold compression strength tests were performed on INSTRON 1195 at a fixed crosshead speed of 10mm min^{-1}. Samples were prepared according to ASTM C133-97 (ASTM C133-97, 2003) and cold crushing strength, modulus of elasticity and absorbed energy of standard and conditioned samples were calculated from the equation:

$$CCS = (\text{Load to fracture})/(\text{Surface area of sample}) \quad (2)$$

The results obtained are presented in Table 3.

Bulk density

The test specimens were dried out at 110°C for 12 hours to ensure total water loss. Their dry weights were measured and recorded. They were allowed to cool and then immersed in a beaker of water. Bubbles were observed as the pores in the specimens were filled with water. Their soaked weights were measured and recorded. They were then suspended in a beaker one after the other using a sling and their respective suspended weights were measured and recorded. Bulk densities of the samples were calculated using the formula below:

$$\text{bulk density} = D/(W-S) \quad (3)$$

where: *D* = Weight of dried specimen, *S* = Weight of dried specimen suspended in water, and *W* = Weight of soaked specimen suspended in air.

The results of this are presented in Table 3.

Water absorption

The test sample was dried out in an oven till a constant weight of the sample was

obtained. The sample was then placed in a vessel containing water in order to be completely submerged without touching the bottom of the vessel in which it is suspended. The vessel was then heated slowly so that the water boileds after heating. After boiling for about an hour with the evaporated water replaced, the sample was allowed to cool at room temperature for 24 hours. The sample was then renamed, blotted and then reweighed. The percentage water absorption was calculated as showed below:

$$\% \text{ water absorption} = (\text{soaked wt} - \text{dried wt})/(\text{dried wt}) \quad (4)$$

Qualitative and quantitative XRD

The samples were prepared for XRD analysis using a back loading preparation method [9, 10]. They were analysed using a PANalytical X'Pert Pro powder diffractometer with X'Celerator detector and variable divergence- and receiving slits with Fe filtered Co-Kα radiation. The phases were identified using X'Pert Highscore plus software. The receiving slit was placed at 0.040°. The counting area was from 5 to 70° on a 2θ scale. The count time was 1.5 s. The temperature-scanned XRD data were obtained using an Anton Paar HTK 16 heating chamber with Pt heating strip. Graphical representations of the qualitative result follow below.

The relative phase amount (weight %) was estimated using the Rietveld method (Autoquan Program) as reported by Young et al. [11]. Amorphous phases, if present, were not taken into consideration in the quantification. The results obtained are presented in Figure 1 and Tables 2 and 4.

X-Ray fluorescence (XRF)

The major elements were determined by X-ray fluorescence with an ARL® 9800 XP spectrometer. The pulverized clay samples were mixed with lithium tetraborate for chemical analysis. The ignition loss was measured by calcinations at 1000 °C. The XRF result is shown in Table 1

Results and Discussions

Table 1 shows the x-ray fluorescence (XRF) semi-quantitative analysis results of the

raw Ifon clay while Figure 1 and Table 2 show the x-ray diffractometry (XRD) results of the raw Ifon clay. Table 3 and Figures 2 to 7 show the various investigated mechanical properties as affected by the different sintering temperatures. Table 4 shows the different phases developed in the various sintered ceramic samples.

Characterization of the raw clay

From Tables 1 and 2 together with Figure 1, the various phase components of the raw Ifon clay are depicted. The major oxide phases (from Table 1 and Figure 1) observed in the raw Ifon clay are alumina (Al_2O_3) and silica (SiO_2), with some hematite (Fe_2O_3), potash (K_2O), magnesia (MgO), calcia (CaO), titania (TiO_2) and soda (Na_2O). Comparing these with Table 2 it is observed that the raw Ifon clay is composed of 5.63% kaolinite, 3.81% muscovite/illite, 30.9% microcline, 18.22% plagioclase/albite and 41.42% quartz. With exception of quartz (which is majorly silica), all other phases depicted in Table 2 are alumino-silicates. This explains the source of the major components of the clay as depicted in Table 1 and Figure 1. It has been reported that various types of clays comprise different clay minerals of the ninety-three planar/non-planar hydrous phyllosilicates [12,13] which are either 1:1 or 2:1 layer type phyllosilicates with/without interlayer water [3, 14].

Table 1. XRF Semi-quantitative analysis of the elements of Ifon clay sample (weight %).

Phases	Weight Percent
Al_2O_3	22.42
SiO_2	63.35
Fe_2O_3	6.109
K_2O	2.878
MgO	1.351
Ba	0.092
CaO	0.689
Cr_2O_3	0.046
Cu	0.021
MnO	0.117
Na_2O	0.789
Ni	0.064
P_2O_5	0.109
SO_3	0.047
Sr	0.019
TiO_2	0.923
Zr	0.045
Total	99.1

Moreover, the feldspar minerals observed in Table 2 (i.e, microcline and plagioclase) explain the source of the oxides of potassium, sodium and calcium as depicted in Table 1 and Figure 1. It has equally been reported that the common impurities in feldspar are iron and titanium [15]; this explains the source of the titania and hematite depicted in Figure 1 and Table 1. The presence of magnesium in the clay is explaine by the presence of muscovite/illite (mica mineral) in the clay. This clay is observed to contain high percentage of feldspar minerals (about 50%), if it is beneficiated could be an important raw material for glass and ceramic industries [16].

Table 2. XRD Result of the Raw Clay Samples Showing the Quantity of Different Phases Present

Phases	Weight %
Kaolinite	5.63
Microcline	30.90
Muscovite/Illite	3.81
Plagioclase/Albite	18.22
Quartz	41.42

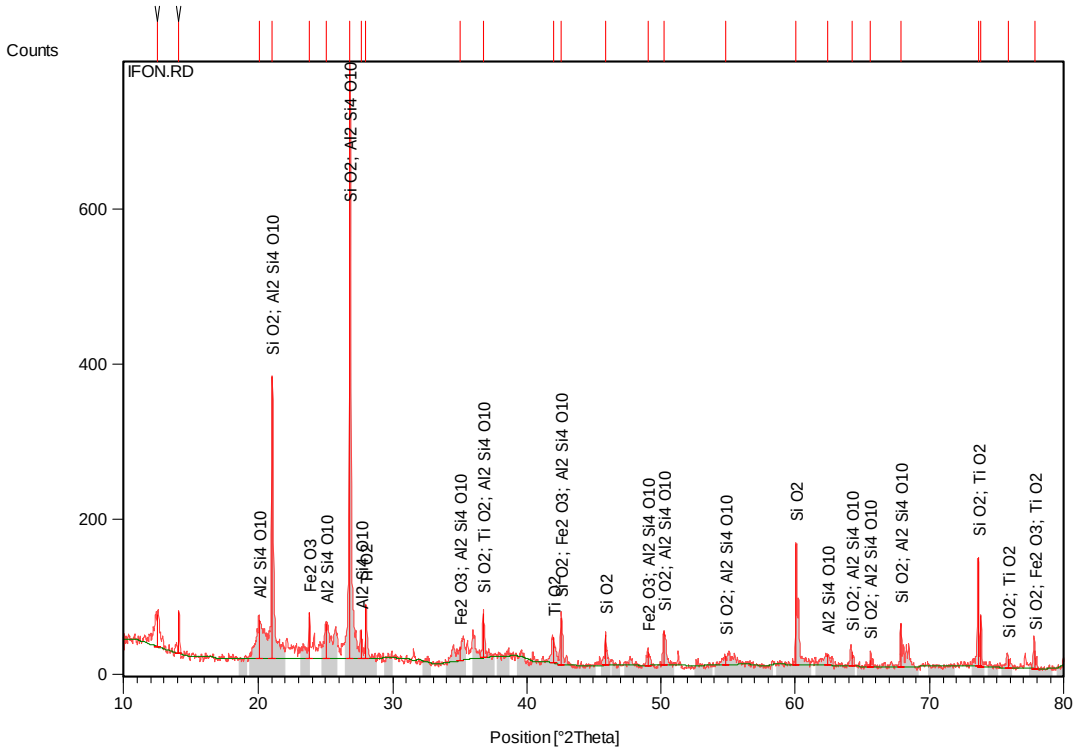

Figure 1. *X-Ray Diffraction Pattern (Phase Analysis) of Raw Clay Sample*

Characterization of the sintered clay based ceramic

The mechanical properties of the sintered clay based ceramic samples is shown in Table 3; Figures 2 to 7 shows the plot of various investigated properties as affected the sintering temperatures, while the various phases in the sintered sample as characterized by the x-ray diffractometry (XRD) is shown in Table 4

Effects of Sintering Temperature on the Mechanical Properties of the clay based Ceramics

Apparent Porosity and Water Absorption

From Table 3 and Figures 2 and 5, the effects of sintering temperature on the apparent porosity and water absorption of the sintered clay based ceramic is vividly shown. It is observed that the apparent porosity of the sintered sample is observed to decrease with increase in sintering temperature. When sample was sintered at 800°C, it has an apparent porosity of 34.46% when the sintering temperature was increased to 900°C its porosity reduced to 31.26%. Further increase in the sintering temperature to 1000°C resulted in further reduction in the porosity of the samples to 28.74% and then to 25.28% at a sintering temperature of 1100°C and lastly to 22.51% at a sintering temperature of 1200°C. This is due to the sintering process; according to Calister, (2007) [17] voids exist between particles of the newly formed green (unfired) ceramic, much of these inter-particles voids are eliminated during firing/sintering to produce sintered ceramic.

Table 3. Showing the Investigated Properties of the Sintered Ceramic as affected by Sintering Temperature

Temperature (^oC)	800	900	1000	1100	1200
Apparent porosity (%)	34.46	31.26	28.74	25.28	22.51
Bulk density (g/cm^3)	2.22	2.24	2.30	2.34	2.36
Water Absorption (%)	41.11	40.11	39.23	37.18	32.44
Thermal shock Resistance	18	18	20	30	30
Cold crushing strength (N/mm^2)	22267	20904	18469	14883	14345
Young's Modulus (N/mm^2)	132419	146348	117805	142490	147881
Absorbed Energy (J)	48.286	36.384	36.978	27.643	27.876

However, it is often the case that this pore elimination process is incomplete and some

residual porosity will remain. A lot of factors determines the amount of these pore that will be eliminated during sintering these include, the temperature at which the ceramic is sintered; the higher the sintering temperature, the higher the amount of the pore that will be filled/eliminated during the sintering operation. Moreover, the composition of the ceramic raw materials from which the ceramic is fabricated together with the sintering temperature equally affects the elimination of the pore during sintering.

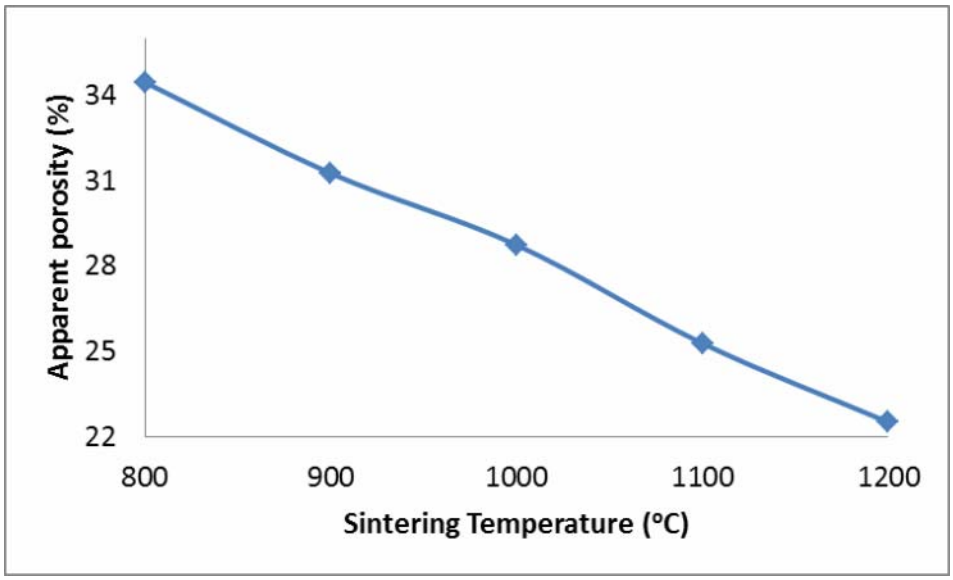

Figure 2. *Effects of Sintering Temperature on the Apparent Porosity of the Samples*

From Table 2 and as discussed above it is observed that the raw Ifon clay contained about 50% feldspar and it has been reported that feldspar minerals favour liquid phase formation and densification at low temperature [8, 18]. The presence of feldspar in the raw Ifon favours the liquid phase sintering of the samples at low temperature.

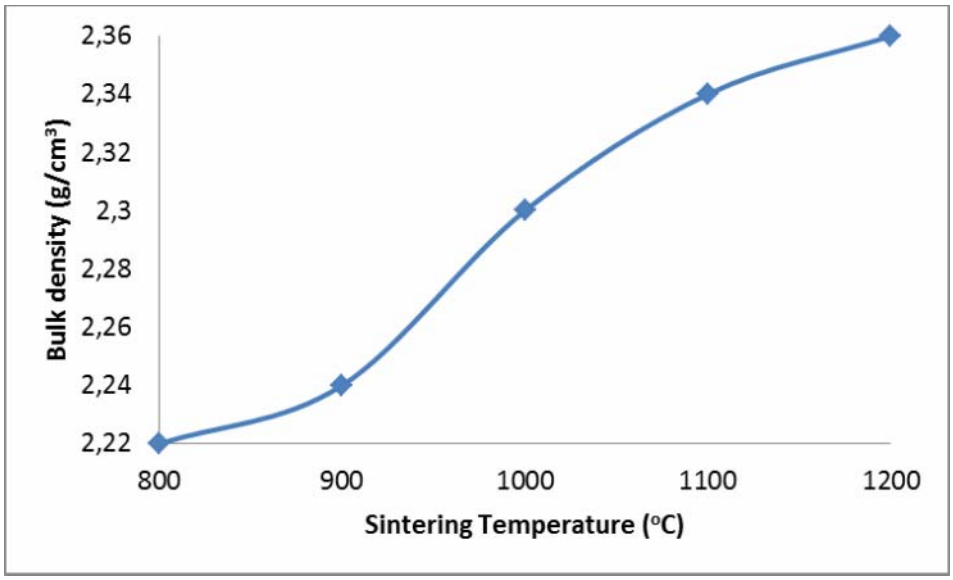

Figure 3. *Effects of Sintering Temperature on the Bulk Density of the Samples*

As the sintering temperature increases from 800°C through different temperatures to 1200°C more liquid phase were increasing formed eliminating more pores with the increase in sintering temperature. This also explains why water absorption the ceramic samples decreased with increased sintering temperature.

Bulk density

From Table 3 and Figure 3 the effect of increase in sintering temperature on the bulk density of the sintered ceramic samples is clearly depicted. Contrary to the relationship which existed between the sintering temperature and the apparent porosity as discussed above, it is observed that the bulk density of the clay based ceramic samples increases with increase in the sintering temperature. This is expected because as the inter-particle voids/pores are progressively filled up with increasing sintering temperature, the volume of the ceramic samples can be said to reduce with increased sintering temperature. This behavior is also due to the reduced porosity of the sample as explained above which lead to increase in the amount of matter in the sample per unit volume [8].

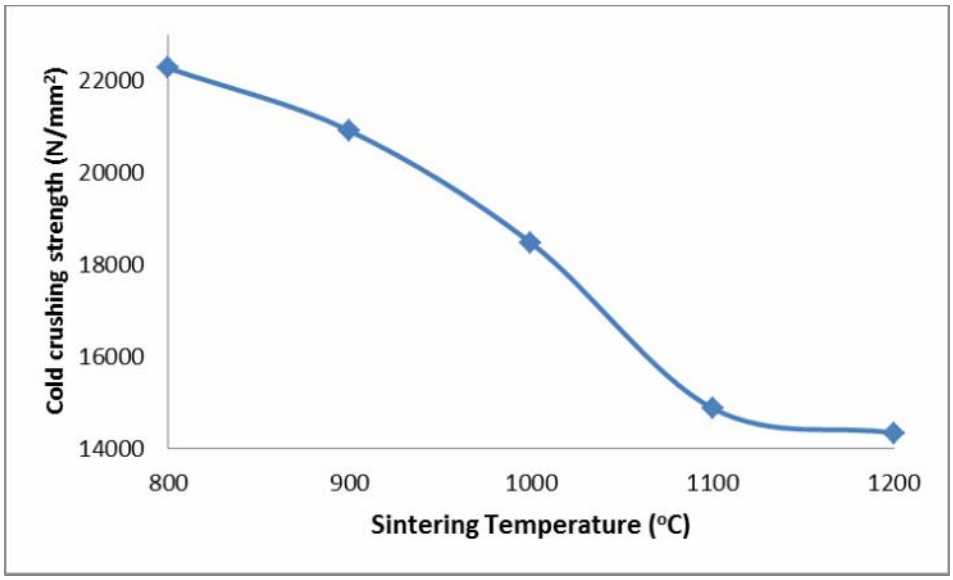

Figure 4. *Effects of Sintering Temperature on the Cold Crushing Strength of the Samples*

Cold Crushing Strength (CCS), Absorbed Energy and Modulus of Elasticity (E)

From Figures 4, 7 and Table 3, the effect of sintering temperature on the cold crushing strength (CCS), and absorbed energy are shown. It is observed that both the CCS absorbed energy of the ceramic samples decreased with increased in the sintering temperature. But as earlier explained, the porosity of the samples reduced with increased sintering temperature, while the bulk density of the samples increased with increased sintering temperature; it would be expected that the CCS of the samples should increased with increased sintering temperature due to an increase in the amount of matter in the sample per unit volume [8, 19]. This abnormal behavior is due to the presence of large content of glassy phase in the ceramic samples as depicted in Table 4. From this Table 4, it is observed that each of the samples contains about 35% feldspar solid solution (microcline and anorthite), which are glass forming components together with silica (quartz). It is a well established fact that glass phase is amorphous (not crystalline), with very high stiffness as it can be seen in Figure 6 that all the samples have very high Young's moduli of elasticity (E). Also it could be generally stated that the Young's modulus (E) increased with increased sintering temperature (with the exception of E at 1000°C where there is a little deviation). Sample QT1 (sample sintered at 800°C) had the highest CCS while all the other samples, even though were sintered at much more higher temperatures, have lower CCS. This is because from Table 4, it is observed that it is only sample QT1 that have the muscovite phase together with all the other phases that other samples also possess. The muscovite could have been able to increase the CCS of the

sample by introducing grain boundaries which served as barriers to the propagation of cracks thereby increasing the breaking/crushing strength of the sample.

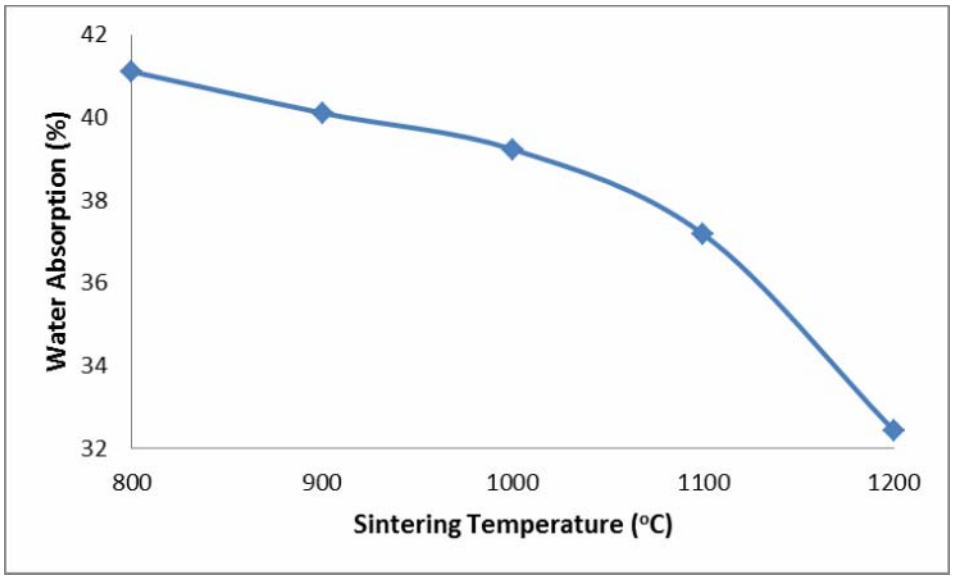

Figure 5. *Effects of Sintering Temperature on the Water Absorption of the Samples*

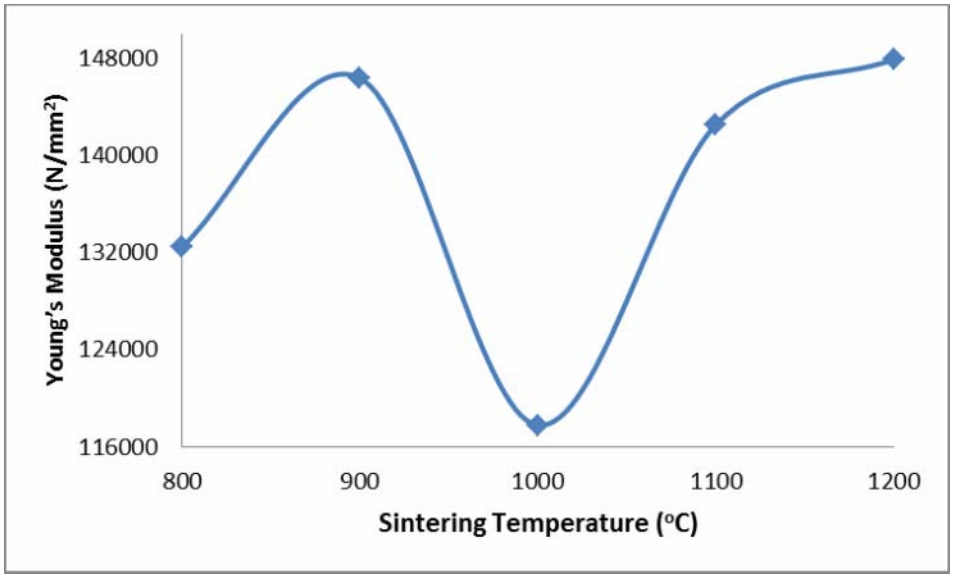

Figure 6. *Effects of Sintering Temperature on the Young's Modulus of the Samples*

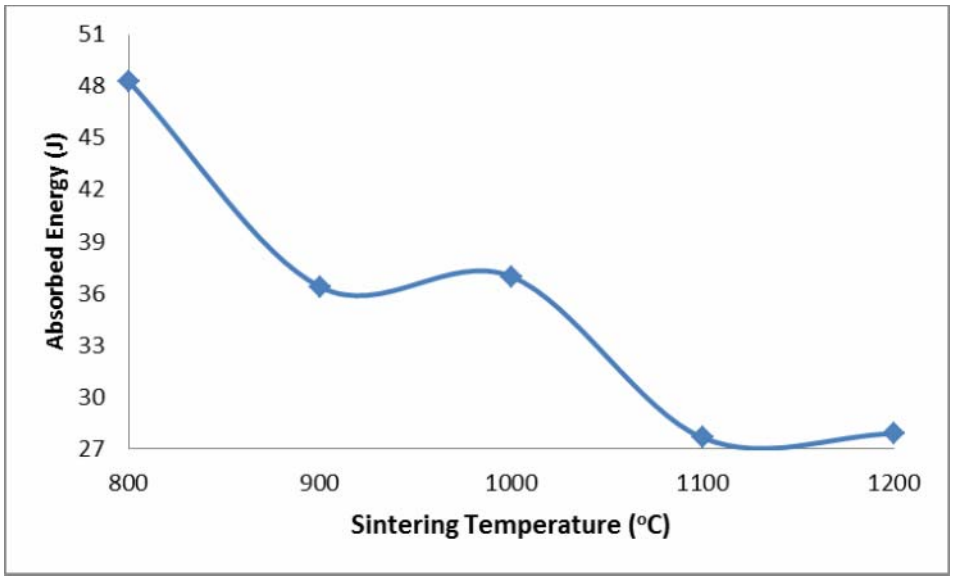

Figure 7. *Effects of Sintering Temperature on the Absorbed Energy of the Samples*

Table 4. X-ray Diffractometry of the Sintered Samples at Various Temperatures

Sample Designation	Sintering Temperature (°C)	Phases (%)			
		Quartz	Microcline	Anorthite	Muscovite
QT1	800	43.76	19.38	14.47	22.39
QT2	900	61.57	22.63	15.80	0
QT3	1000	65.71	19.51	14.78	0
QT4	1100	66.91	18.09	15.00	0
QT5	1200	64.22	20.21	15.57	0

From Table 4, it is observed that the muscovite was observed in the sample that was sintered at 800°C, while the muscovite phase was conspicuously missing in the samples sintered at higher temperatures. This is not unconnected with the dehydroxylation muscovite undergoes when subjected to sintering at high temperatures [20,21,22], However, the dehydroxylation progresses from 800°C upto 1140°C [22], but it is completed in these samples at 800°C. This is because of the presence of other phases (such as feldspar; microcline and plagioclase) in the samples that interracted the dehydroxilation reaction and assisted it to be completed at 800°C.

Conclusions

From the discussion, it is concluded that;

a. the Ifon clay deposit is feldspathic; it contains about 50% feldspar;

b. apparent porosity, cold crushing strength, absorbed energy and water absorption of the samples decrease with increased sintering temperature;
c. bulk density and Young's Modulus of elasticity of the samples increased with increased sintering temperature
d. the sintered samples composed mainly of quartz, microcline and anorthite, only the sample sintered at 800°C contains muscovite; and
e. sample QT1 (sintered at 800^{o}C, held for 1 hour and cool in the furnace) is considered the optimum.

Acknowledgements

The author will like to appreciate the assistance rendered by the Head, Department of Materials Science and Engineering for the permission granted to make use of their laboratory facilities.

References

1. Mortland M., Shaobai S., Boyd S., Cl*ayorganic complexes as adsorbants for phenols and chlorophenols*, Clays and Clay Minerals, 1986.
2. Burch R., Warburton C., *Pillared Clay as Demetallisation Catalysts*, Applied catalyse, 1987.
3. Aramide F.O., *Effect of Firing Temperature on Mechanical Properties of Fired Masonry Bricks Produced from Ipetumodu Clay*, Leonardo Journal of Sciences, 2012, 21, p. 70-82.
4. Dananaj I., Frankovska J., Janotka I., *The influence of smectite content on microstructure and geochemical properties of calcium and sodium bentonites*, Appl. Clay Sci., 2005, 28, p. 223-232.
5. Akwilapo L. D., Wiik K., *Ceramic Properties of Pugu Kaolin Clays, Part 2: Effect of Phase Composition on Flexural Strength*, Bull. Chem. Soc. Ethiop., 2004, 18(1), p. 7-16.
6. Martín-Márquez J., Rincón J. Ma. and Romero M., *Effect of firing temperature on sintering of porcelain stoneware tiles*, Ceramics Internacional, 2007, 34(2008), p. 1867-1873.

7. Johari I., Said S., Hisham B., Bakar A., Ahmad Z. A., *Effect of the Change of Firing Temperature on Microstructure and Physical Properties of Clay Bricks from Beruas (Malaysia)*, Science of Sintering, 2010, 42, p. 245-254.
8. Aramide F. O., *Production and Characterization of Porous Insulating Fired Bricks from Ifon Clay with Varied Sawdust Admixture*, Journal of Minerals and Materials Characterization and Engineering, 2012, 11, p. 970-975.
9. Aramide F. O., Alaneme K. K., Olubambi P. A., Borode J. O., *Characterization of some clay deposits in South West Nigeria*, Leonardo Electronic Journal of Practices and Technologies, 2014, 25(2), p. 46-57.
10. Kleeberg R., Monecke T., Hillier S., *Preferred orientation of mineral grains in sample mounts for quantitative XRD measurements: How random are powder samples?*, Clays and clay minerals, 2008, 56 (4), p. 404-415.
11. Young R. A, Sakthivel A., Moss T. S., Paiva-Santos C. O., *Rietveld analysis of X-ray and neutron powder diffraction patterns*, School of physics, Georgia Institute of Technology, 1994, Atlanta, U.S.A..
12. Bergaya F., Theng B. K. G., Lagaly G., *Development in Clay Science*, Handbook of Clay Science, Elsevier Ltd., 2006.
13. Guggenheim S., Adams J. M., Bain D. C., Bargaya F., Brigatti M. F., Drits V. A., Formoso M. L. L., Galan E., Kogure T., Stanjek H., *Summary of the recommendations of nomenclature committees relevant to clay mineralogy: report of the Association International pour l'Etude Argiles (AIPEA)*, Nomenclature Committee for 2006, *Clay Minerals*, 2006, 41, p. 863-877.
14. Bailey S. W., *Summary of recommendation of AIPEA nomenclature committee on clay minerals*, Am. Mineral., 1980, 65, p. 1-7.
15. Saklar S., Oktay C., Karadeniz M., Gürsu S., *Feldspar Beneficiation from Manisa Alaşehir Pegmatites*, TS"1 International Mining Congress and Exhibition of Turkey-IMCET 2003, 2003, pp. 457-459.
16. Bayraktar I., Çakır U., Quality Feldspar Production at Çine Akınaden. *Industrial Minerals*, May, 2002, pp. 56-59. Callister, William D., Materials Science and Engineering: An Introduction, 7th Edition, *John Wiley & Sons, Inc*, 2007, pp. 451
17. Ergul S., Akyildiz M., Karamanov A., *Ceramic Ma- terial from Basaltic Tuffs*, Industrial Ceramics, 2007, 27(2), p. 89-94

18. Norton F. H., *Refractories*, McGraw-Hill, 4th Edition, New York, 1968.
19. Grim R. E., Bradley W. F., Brown G., In : *X-ray Identification and Crystal Structures of Clay Minerals*, ed. G. W. Brindley. Mineralogical Society, London, 1951, pp. 138-172.
20. Gridi-Bennadji F., Beneu B., Laval J. P., Blanchart P., *Structural transformations of muscovite at high temperature by X-ray and neutron diffraction*. Applied Clay Science, 2008, 38(3-4), p. 259-267.
21. Gridi-Bennadji F, Chateigner D, Di Vita G, Blanchart P. *Mechanical properties of Textured ceramics from muscovite–kaolinite alternate layers*, Journal of the European Ceramic Society, 2009, 29 p. 2177-2184.